



Historical earthquakes, tsunamis and real-time earthquake monitoring for tsunami advisory in the South China Sea region

Zhiguo Xu, et al. [*full author details at the end of the article*]

Received: 16 July 2020 / Accepted: 23 January 2021 / Published online: 11 February 2021
© The Author(s), under exclusive licence to Springer Nature B.V. part of Springer Nature 2021

Abstract

The South China Sea Tsunami Advisory Center (SCSTAC) established by China, under the aegis of UNESCO's Intergovernmental Oceanographic Commission (UNESCO/IOC), had inaugurated commencing its full operation on November 5, 2019. This center is operating 24×7 h and round-the-clock shift to monitor tsunami hazard that pose a serious threat to countries which bordering the South China Sea (SCS) region. Prior to the official operation, SCSTAC had taken action for the last 10 years in upgrading their technology capability which are real-time earthquake monitoring and the processing system that is crucial to be able providing the international standard of tsunami warning services in the SCS and its adjacent areas. This paper briefly reviewed on the initiation steps and its developments of the South China Sea region Tsunami Warning and Mitigation Systems, tectonic setting as well as the characteristics of historical earthquakes and tsunamis in the region. In addition, we highlighted the structure and basic functions of the earthquake monitoring and processing system, earthquake location, source mechanism solution and finite fault model inversion using the real-time seismic waveform data from regional and global seismographic networks that will result in the rapid source parameters estimation for a larger earthquake in tsunami warning. Numerous simulations and hands-on events have shown that the preliminary earthquake parameters could be determined less than 8 min after earthquake. The W phase method is used and be able to produce rapid and reliable estimation of the moment magnitude and source mechanism for larger events within 10–15 min from earthquake origin time. A finite fault model can be acquired just after the earthquake event via computing teleseismic body-wave inversion program. The earthquake monitoring and processing system provide accurate and reliable information in contributing to tsunami warning services, thus promoting the development of tsunami warning technologies, which enhancing the tsunami warning capability and tsunami emergency responses. These high-end technology can be used in facilitating others such as marine disaster prevention, mitigation and its risk reduction.

Keywords South China Sea region · Tsunami warning · Preliminary earthquake parameters · Focal mechanism · Finite fault model · Tsunami simulation

1 Introduction

On December 26, 2004, a M_w 9.0 (Harvard CMT) earthquake rumbled in the deep in the sea off the coast of Northern Sumatra, Indonesia. The giant tsunami was generated from the earthquake, and it prompted immediate warning around the world that claimed more than 283,100 people and caused destruction to the surrounding as the waves sped out across Indian Ocean (Athukorala and Resosudarmo 2005; Wang and Liu 2006). There was an unprecedented response to the disaster. It has drawn quick responses and attentions from nearby local communities to react first, mobilizing whatever resources they had, followed by fast national responses and later a huge global responses including China.

The SCS and its surrounding areas are situated at the boundaries of three major plate: Eurasian, the Pacific and the India–Australia. The convergence of these plates has resulted in frequent occurrence of complex tectonic regime in the region such as earthquakes, volcanic activities and tsunamis. This region covers not only the SCS but also its adjacent basins, Sulu Sea and Celebes Sea (Sulawesi Sea), and is characterized as one of the most vulnerable regions to major tsunamigenic earthquakes due to the high seismicity of the Manila Trench, Cotabato and Negros Trench and North Sulawesi Trench (Liu et al. 2009; Baeda 2011; Mardi et al. 2017). When a catastrophic tsunami occurs, it could pose great threat to the coastal areas of the neighboring countries in the region.

To adequately address the risk of tsunamis in the SCS region, IOC Executive Council 41st Session in 2008 (EC-XL1.6) had urged Member States of the region and other regional seas, to aggressively promote the development, establishment and keeping up the national operation and subregional Tsunami Warning and Mitigation Systems within the framework of Intergovernmental Coordination Group for the Pacific Tsunami Warning and Mitigation System (ICG/PTWS). The 23rd session of ICG/PTWS held in Samoa in 2009 had formed South China Sea Regional Working Group in order to facilitate constructing the system in this region through regional cooperation. In 2011, China officially submitted layout building plan for Tsunami Warning and Mitigation System in the South China Sea Region during the 24th ICG/PTWS session in Beijing. The 25th ICG/PTWS session hosted in Vladivostok, Russia, in 2013 officially reached an agreement on the establishment of the UNESCO's Intergovernmental Oceanographic Commission (UNESCO/IOC) South China Sea Tsunami Advisory Center (SCSTAC), which build upon China's National Marine Environment Forecasting Center (NMEFC). On January 26, 2018, under the approval of IOC, The SCSTAC officially started its trial operation. The 28th session of the ICG/PTWS 28th took place in Nicaragua in March 2019, on 5 November decided to begin full operation of SCSTAC. The SCSTAC provides tsunami monitoring and warning services 24×7 to the countries surrounding SCS region. If any underwater earthquake with magnitude greater than or equal to 6.0 occurs in the South China Sea region, tsunami warning bulletin could be promptly announced to the neighboring countries that rely on communication via fax, website, email and the Global Telecommunication System (GTS). The SCSTAC Area of Service (AoS) specified by ICG/PTWS covers all the coasts of the South China Sea and the adjacent Sulu Sea and Celebes Sea, with a total of 9 countries bordering the SCS including China, Brunei, Cambodia, Indonesia, Malaysia, the Philippines, Singapore, Thailand and Vietnam (Fig. 1).

The South China Sea Tsunami Warning and Mitigation System, led by the IOC and assisted by the countries in the SCS, has been established with the potential to develop and establish its own independent and original information, knowledge and technology. The tsunami warning system integrates the real-time earthquake and sea-level monitoring



Fig. 1 Area of Service for South China Sea Advisory Center. The shade region of deep blue shows the SCSTAC Area of Service (AoS) specified by ICG/PTWS, it covers all the coasts of the South China Sea and the adjacent Sulu Sea and Celebes Sea, and red dots endnote the major cities surrounding SCS region

system, tsunami scenario database, real-time tsunami model forecasting system, as well as generating and dissemination of tsunami advisories and so on. This system could provide tsunami warning services for China, the SCS region and other by tsunami hazard within 10 min after earthquake.

The tsunami warning system uses the physical principle that seismic wave travels more quickly than tsunami wave with a factor of 10 to 50, so the initial tsunami warnings are made based on rapid detection and seismic activity characterization in order to reduce tsunami damage, allowing people on the coast more time to respond and prepare it. Today, tsunami warning center relies mainly on real-time seismic stations installed worldwide and monitors the activity of undersea earthquake in order to quickly determine the preliminary earthquake parameters: origin time, epicenter, magnitude, focal depth, geometry of focal mechanism and the rupture area after the time of the earthquake. The tsunami duty officers need to make prompt decision based on earthquake information and to issue the qualitative or quantitative tsunami warning products. Thus, the real-time earthquake monitoring

system plays an important role in tsunami warning. In generally, a tsunami warning system includes two stages: The first stage consists in the determination of the earthquake sources parameters (location, magnitude, focal mechanism solutions, finite fault solutions) and the second stage is dependent on the tsunami wave propagation forecast with the tsunami numerical calculations. In this paper, we mainly focus on the structure and core functions of the real-time seismic monitoring and processing system in SCSTAC in the context of tectonic setting of the South China Sea and neighboring areas and the historical earthquakes and tsunamis activities, in order to provide tsunami warning information for the swift and accurate earthquake event after the earthquake.

2 Historical earthquakes and tsunamis in the South China Sea region

2.1 Regional tectonic setting

Tectonically, the SCS areas is situated on the threefold crossroads of southeast Asia between the Eurasia Plate (EP), Indo-Australia Plate (IA) and Philippine Sea Plate (PSP) and being dominated by the interactions of these plates. South China Sea is on the small tectonic plate of Sunda Block, which is once called the southeast of the Eurasia Plate before been separated by a distinct moving direction from India–Eurasia continental collision (Cardwell and Isacks 1978; Johnston and Bowin 1981; Simons et al. 1999, 2007; Michel et al. 2000; Bird 2003). The Sunda Plate travels northeast based on GPS measurement relative to Eurasia at a pace of approximately 10 mm/yr (Socquet, et al. 2006). On the eastern side, the PSP is moving approximately 70–80 mm/y northwestward (Kreemer et al. 2000). The Philippine Mobile Belt, Molucca Sea Collision Zone, Molucca Sea Plate (MSP), Banda Sea Plate and Timor Plate are the boundary of Sunda with extreme tectonic patterns on the east. The Indo-Australia Plate is located in the south and west of Sunda Plate and moves north at a rate of approximately 40–50 mm/y, subducting under a portion of the Eurasia Plate, creating the Sunda Trench and a large fault called an interplate thrust under the Sunda Plate (Lin et al. 2014). In 2004, the Sumatra M_w 9.0 megathrust earthquake took place on the platform of subduction region, producing an unparalleled devastating tsunami. The Sunda Plate is situated north of the plateau of Burma, Eurasian Plate and Yangtze Plate. Overall, the Sunda Plate's east, south and west boundaries are tectonically complex and seismically active; only the northern boundary is relatively quiet.

The collision of three plates induces a large degree of complicated tectonic stress in SCS. On the east side of SCS region, the convergence resulted to several subduction zones marked by oceanic trenches, which includes the Manila Trench (MT) in the north, the Negros Trench (NT) in the central Philippines, the Sulu Trench (ST) and Cotabato Trench (CT) in the south, and the North Sulawesi Trench (NST) in the southeastern (Cardwell et al. 1980). The Sunda Plate subducts eastward through a network of pits, followed by a significant number of small, intermediate source earthquakes.

The oceanic lithosphere of SCS is consumed underneath the Manila Trench, which is east-dipping and nearly N–S striking subduction zone, starting from the north end of tip of Palawan, the Philippines, developing to the north of the western bank of Luzon in the Philippines and reaching Taiwan by a total length of about 1000 km. The water depth of the subduction zone lies between 4800 and 4900 m with the deepest of Manila Trench reaching 5400 m (Megawati et al. 2009; Xie et al. 2019; Liu et al. 2015). In addition, the submerged topography is complex and there are a large number of north–south direction

seamounts parallel to the trench. The depth of water and the topography of the trench area fluctuate considerably, so the conditions for earthquake and tsunami generation are fulfilled. The Manila Trench (MT) is considered to be the most potential source of devastating tsunamis (Kirby et al. 2005; Liu et al. 2009; Mardi et al., 2017).

Due to the Sulu Sea oceanic lithosphere subducts underneath the Negros–Zamboanga–Sulu–Jolo Arcs (Aurelio et al. 2017), two main subduction zones of the Negros Trench (NT) and the Sulu Trench (ST) exist in the Sulu Sea, which are considered as more hazardous sources to the tsunami generation. The Negros Trench (NT) is a long trendy N–S fault line with eastern dip, running from Mindanao to Panay, and passing southwest of Negros Island. Sulu Trench is in the south of the Philippines, close to Mindanao Island. The size and position of this trench are believed to have the potential to generate tsunamis especially in the coastal areas facing Sulu Sea. Previous studies have shown that the location and size of the two trenches are wide enough to create a massive tsunami with the greatest impact on the Sulu Sea coastline (Aziz et al. 2011; Mardi et al. 2017).

There are two trenches in the Celebes Sea region. A trench called The North Sulawesi Trench (NST) lies along the base of the continental slope along the north side of Sulawesi. The NST ends at the east where the northeast tip of the North Arm of Sulawesi swing from an easterly trend to a northerly one. Another trench, Cotabato Trench lies off the southwestern coast of Mindanao in the Philippines, which is east-dipping subduction that crosses the Celebes Sea and the Moro Gulf in Southern Mindanao, where the Celebes Sea oceanic lithosphere underplates the Sarangani–Sangihe Arcs (Aurelio et al. 2017).

2.2 Historical earthquakes and tsunamis

Given the special geographical location of the SCS and its surroundings, geological disasters such as earthquakes, tsunamis, volcanic eruptions are frequent. We collect the NEIC earthquake catalogs list from 1900 to 2019 in the studied area (-7 to 32°N , 95 – 13°E). Figure 2a shows the cumulative frequency of earthquakes with magnitude no less than 4.5 in and around the South China Sea. The lower level of seismic monitoring technology and the sparse seismic stations resulting in the total number of recorded earthquakes were only 1911 during the years of 1900–1975. In the following period, as seismic observation technology rapidly evolved, the stations shifted to digital recording, the station's distribution density increased significantly, and the number of recorded earthquakes showed exponential growth which provides abundant observational data for earth science research. The frequency distribution of earthquake magnitudes is shown in Fig. 3b. The figure shows 26,517 earthquakes of magnitudes ranging between 4.5 and 4.9. There were 12,033 earthquakes with magnitude 5–5.9, 1,405 earthquakes of magnitude 6–6.9, 213 earthquakes with magnitude 7–7.9 and 13 earthquakes recorded with magnitude 8 and above. The depth frequency distribution of the earthquake source shows that (Fig. 2c) shallow, intermediate and deep earthquakes are distributed, with 29,713 shallow earthquakes (< 70 km), 9,283 intermediate earthquakes (70–300 km) and 1185 deep earthquakes (> 300 km), accounting for 73.9%, 23.1% and 3.0% of all earthquakes, respectively.

We can see from the distribution of the earthquakes in SCS and the adjacent region with clear spatial distribution characteristics (Fig. 3). The earthquakes are clustered in the subduction zone on the western edge of the Circum-Pacific belt, along the Japanese Ryukyu island arc, Chinese Taiwan island arc and the Philippine island arc, extending from north to south, until the Indonesia archipelago, and consistent with the strike of the major subduction zones. Most of the earthquakes above magnitude 7 are concentrated in the narrow

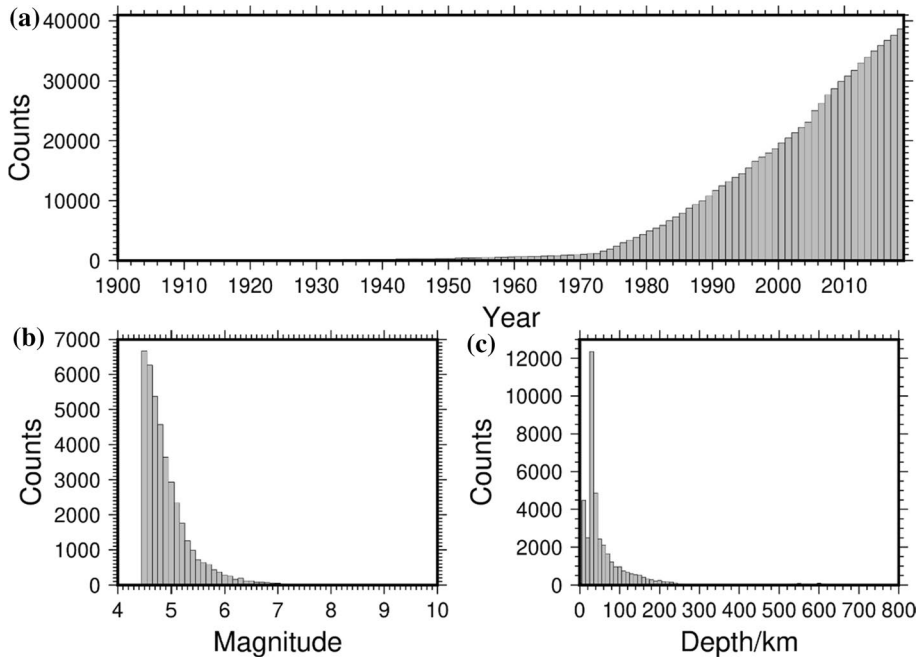


Fig. 2 a Cumulative frequency of earthquakes, b magnitude frequency, c depth frequency

zone between plates, and the subducted plates generate high-level frequent and strong earthquakes. In contrast, earthquakes are rare in the northern side of the South China Sea, but many earthquakes of magnitude 7 or above have occurred in history under the interaction of the active Qiongyue coastal fault system (Yang and Lin 1990). There are few earthquakes in the central region of the South China Sea with magnitude less than 6.0. Clearly, the focal depth of the SCS and its adjacent areas is not uniform. Shallow earthquakes are mainly spread near the outer edge of the island arc, within the subduction zone and the continental margin orogenic belt, such as the Philippine Mobile Belt. Most of the intermediate earthquakes are mainly distributed in the direction of major subduction zones such as the Manila Trench (MT), the Negros Trench (NT), the Sulu Trench (ST), the Cotabato Trench (CT) and the Philippine Trench (PT). The focal depth gradually increases as far away from the trench, the deepest depth earthquakes associated with the maximum depth of subduction. Deep-focus earthquakes often occur in the south of 9° N, mainly in the Sulawesi Sea region with a maximum depth up to 678 km, which is caused by the subduction of the Molucca Sea Plate under the Sunda Plate.

Tsunamis are typically triggered by undersea earthquakes, volcanic eruptions, marine landslides or climate changes, most of which are caused by marine earthquake. We integrate the global historical database from the US National Geophysical Data Centre (NDGC) and the Novosibirsk Tsunami Laboratory (NTL) to detail the characteristics of earthquake-generated tsunami sources in the South China Sea region and adjacent. We exclude lower tsunami validity with erroneous entry = 1 and extreme disturbance in inland rivers = 0 in the study region domain ($7\text{--}32^{\circ}\text{N}$, $95\text{--}132^{\circ}\text{E}$). We pick up earthquake-related including (1) earthquake, (2) questionable earthquake, (3) earthquake and landslide, (4) volcano and earthquake, and (5) volcano, earthquake and landslide, to examine

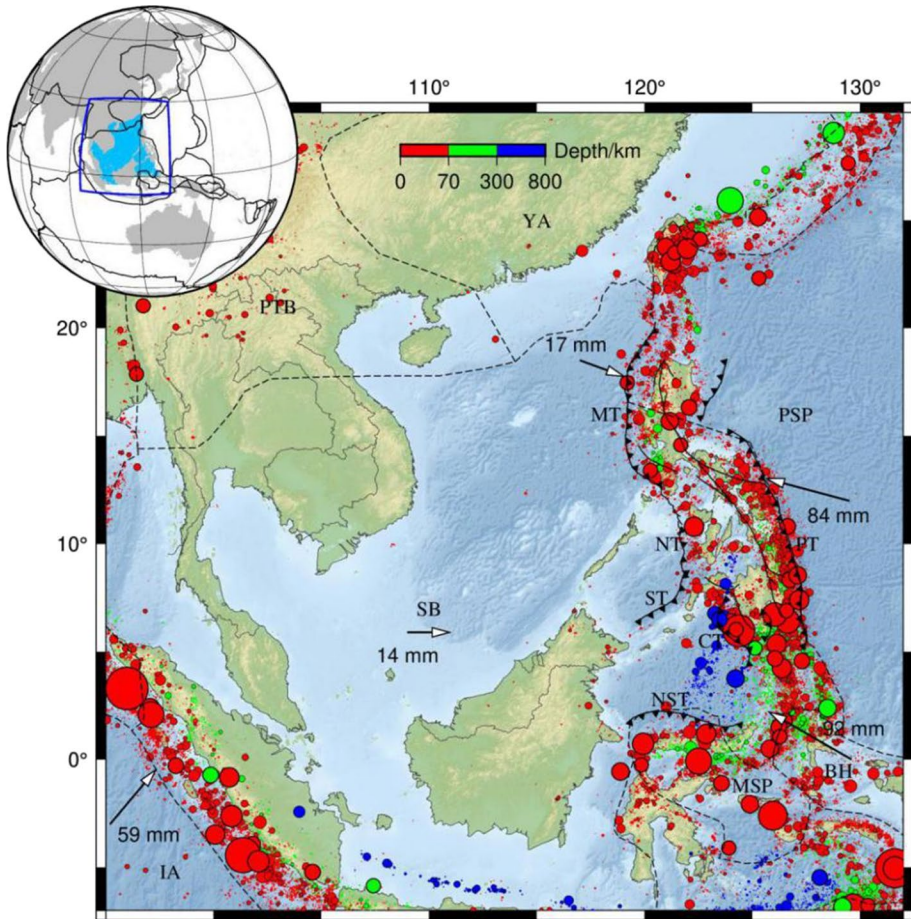


Fig. 3 Overview of regional tectonic setting and historical earthquakes in the South China Sea region. The black dash lines denote the main plate boundary (PSP, Philippine Sea Plate; SB, Sunda Block; IA, Indo-Australia Plate; YA, Yangtze Plate; PTB, Permian–Triassic Boundary; MSP, Molucca Sea Plate; BH, Bird’s Head Plate), the teeth lines are the main trenches (MT, Manila Trench; NT, Negros Trench; ST, Sulu Trench; NST, North Sulawesi Trench; PT, Philippine Trench), and the arrows indicate the subduction direction of the plate, while historical earthquakes are shown as colored circles, and circle dimensions proportionate to the magnitude and the color represents the depth

earthquake-related sources distribution characteristics. The integration of the tsunami catalog and Harvard GCMT solution from 1976 to 2019 collected the focal mechanism solutions of the subsequent tsunamigenic earthquakes, and identified the fault type with triangle diagram (Frohlich 1992) and analyzed the focal mechanism solution characteristics of the tsunami earthquake in this area.

Figure 4 shows the past tsunami-related earthquake and their focal mechanisms in the South China Sea and neighboring regions. According to the spatial distribution of tsunami events, the tsunami sources are near to the coastline and primarily concentrated along the arcs and trenches of the islands, which is usually consistent with the spatial distribution characteristics of historical shallow earthquakes. Most tsunamis are caused by shallow earthquakes with focal depths ranging from 10 to 25 km. Most tsunami-generated

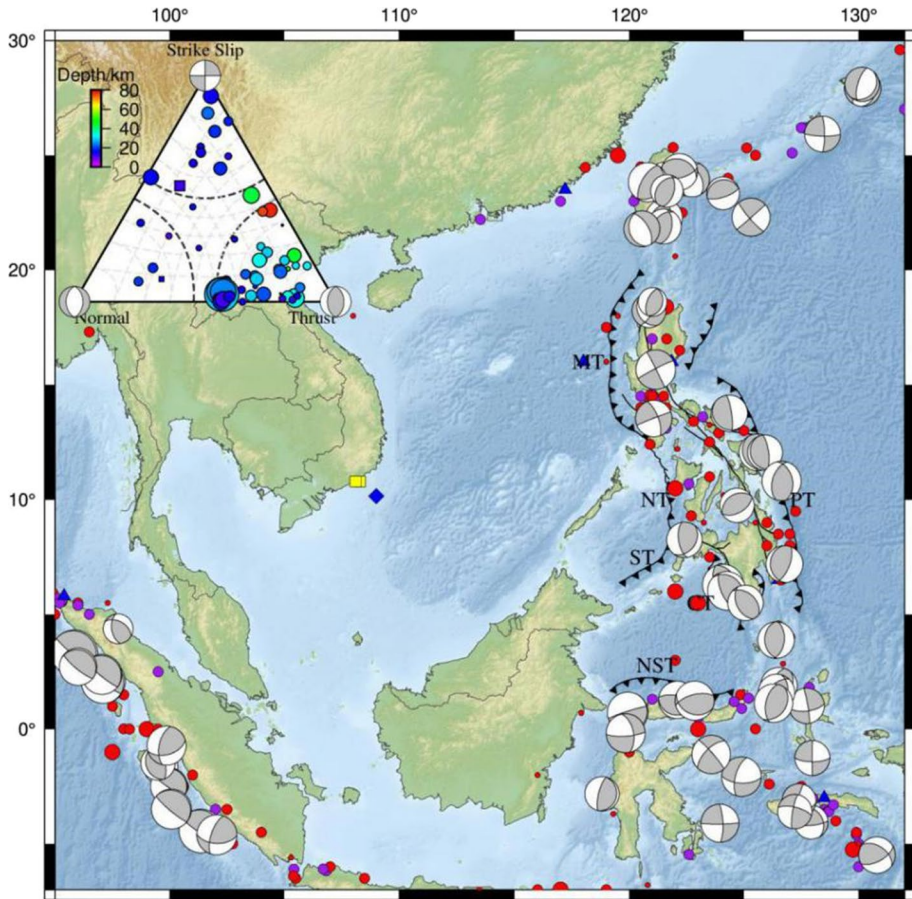


Fig. 4 Regional historical tsunamis in the South China Sea and adjacent areas and focal mechanism solutions of tsunamigenic earthquakes. The teeth lines are the main trenches around the SCS and its surrounding areas, the same as Fig. 2. The various symbols denote the earthquake-related historical tsunami (circles, earthquake; squares, questionable earthquake; triangles, earthquake and landslide; diamonds, volcano, earthquake and landslide). The inset shows the distribution of the tsunamigenic earthquakes with focal mechanism solution by ternary diagram, the sizes of circle scale with earthquake magnitude, and their color with its depth

earthquakes are above 6.0 in magnitude representing 95.1% of all known earthquake magnitude.

Figure 4 also shows the distribution of the 59 tsunamigenic earthquakes with focal mechanism solutions by ternary diagram to assess the type of earthquake sources: Thrust fault (40) accounts for 67.8% of all data, and strike–slip (11) accounts for 18.7%, and normal fault (5) accounts for 8.5%, others are unknown. The findings show that the tsunamigenic earthquakes are typically thrust faults, and a small amount of earthquakes with strike–slip and normal faults may also cause tsunami. A tsunami can be generated when a thrust earthquake causes the seafloor to unexpectedly deform vertically. The Sumatra M_w 9.0 earthquake-generated tsunami on December 26, 2004, the eastern coast of Honshu, M_w 9.0 earthquake tsunami on March 11, 2011, which are typical tsunamis that caused by thrust faults related earthquakes (Lay 2005; Paras-Carayannis 2013). The strike–slip

earthquake usually causes horizontal dislocation on both sides of the fault, and there is no apparent uplift and subsidence in vertical direction, which does not typically result in a massive tsunami, but that does not mean the strike–slip earthquake does not generate tsunami. The large strike–slip earthquakes sometimes trigger landslides and submarine slumps, and then produce major tsunami. On November 15, 1994, the M_W 7.1 Mindoro strike–slip earthquake triggered a tsunami that killed 33 people. A shallow, large earthquake hit the Sulawesi of Indonesia on September 28, 2018, following the main shock, a localized tsunami struck Palu and resulted in the death of 2245 people. The post-tsunami investigation suggests that the underwater landslide and submarine lumps triggered by the strike–slip earthquake caused secondary tsunami (Imamura et al. 1995; Syamsidik et al. 2009). Similarly, tsunami may also be produced from landslides near the active normal fault. On October 18 and 19, 1995, in Amami-Oshima-Kinkai, Japan, the two successive earthquakes with magnitudes 7.1 and 6.8 occurred, which were normal fault earthquake that induced tsunami with maximum tsunami wave heights of 2.59 m and 1.5 m, respectively. A 7.1 normal fault earthquake occurred in Hengchun, Taiwan, on December 26, 2006, also caused a minor tsunami.

Figure 5 shows the distribution of maximum tsunami wave height in the South China Sea and adjacent regions caused by earthquake-generated tsunami sources. The color scheme is based upon the Pacific Tsunami Warning Center (PTWC) alert criteria. Blue, yellow, orange and red color represent maximum tsunami wave height ≤ 0.3 m, 0.3–1 m, 1–3 m and > 3 m. As can be seen from the figure, most tsunamis created by earthquake cause the maximum tsunami wave height to exceed 0.3 m, accounting for 73.6% of the

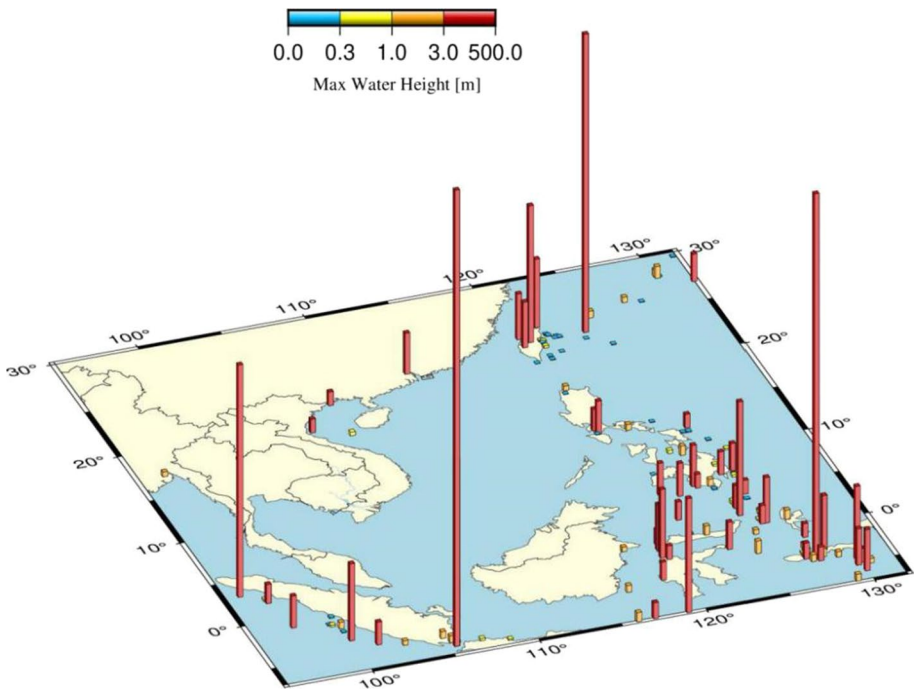


Fig. 5 Distribution of maximum tsunami wave height

total. The tsunami sources particularly lie in the Taiwan Strait and its northeast side, the southwest of Luzon island and most of the coastal areas of the Sulawesi Sea lead to maximum tsunami wave height more than 3 m, suggesting that the South China Sea and its adjacent areas have the conditions for large-scale tsunami, and the possible tsunami danger in those areas is very high.

3 Real-time earthquake and tsunami monitoring for tsunami advisory

3.1 Regional and global seismic networks

Seismic network is one of the most important components of tsunami warning system primarily used to monitor the regional and global undersea earthquakes, and to quickly evaluate seismic and source-type parameter based on real-time seismic waveform data from station all over the world. The rapid detection and characterization of tsunami-generating earthquakes provide the first indication of a potential tsunami.

In order to enhance earthquake monitoring capability in the offshore region of China, 28 broadband seismic stations in marine environmental observation stations have been introduced by the State Oceanic Administration (SOA) and rely on the availability of resources. All these stations were equipped with BBVS-120 broadband seismometer and 24-bit data loggers with high dynamic range which produced by Beijing Gangzhen Instrument and Equipment Co., LTD, which real-time seismic data continuously delivered to SCSTAC with dedicated cable. In addition, 54 broadband seismic stations were acquired from China Earthquake Administration (CEA) and processed in the real time and stored in tsunami warning center. The seismic stations from CEA and SOA via SeedLink communication server constitute a regional seismic network to monitor the undersea earthquakes occurring at China's offshore and the SCS region.

Since these regional stations are concentrated over the coastal areas of the southeast China and not well distributed in azimuth for the earthquakes outside the network, the most reliable earthquake positions are difficult to locate. Therefore, seismic streams from 560 stations from major seismic data centers, including IRIS/DMC, GEOFON, GEOSCOPE which worldwide distributed, are acquired in real time and integrate with region network (Fig. 6). A global network for monitoring submarine earthquake might occur over China's offshore, the SCS and other regions. The global seismic stations provide powerful waveform data for rapid earthquake location, near real-time determination for focal mechanism and finite fault model.

3.2 Real-time sea-level monitoring networks

The real-time tide gauge stations along the coastline and deep-ocean tsunami detection buoys are one of the main instruments for monitoring tsunami. The sea-level data can effectively determine whether a tsunami has occurred, as well as the intensity and magnitude scales for tsunami. The SCSTAC monitors in real time more than 600 sea-level and deep-ocean instruments from around the world for tsunamis. The data are collected by WMO's Global Telecommunication System (GTS), the IOC IODE Sea-Level Monitoring facility, and FTP server from member states of SCS. Two deep-ocean tsunami buoys deployed by China in the west side of Manila Trench of SCS after Indian Ocean tsunami occurred in 2004 (Zhao et al. 2013). However, due to the prolonged exposure to vandalism,

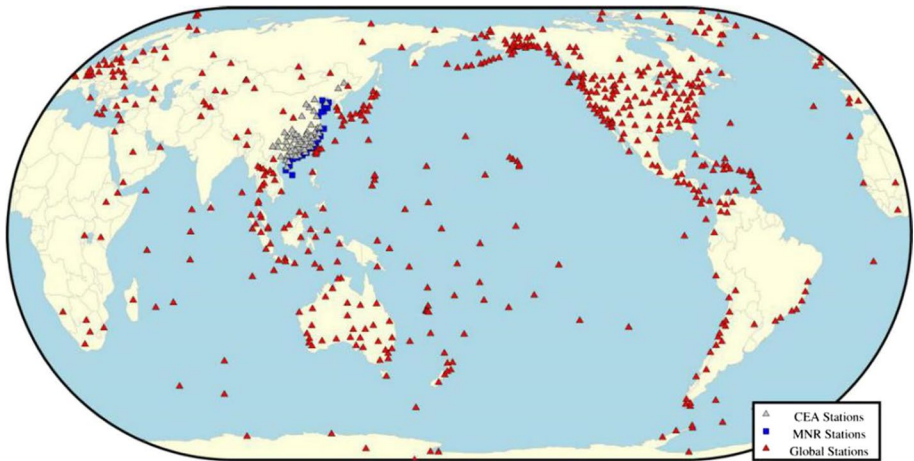


Fig. 6 Regional and global seismic stations for tsunami warning service. The stations are marked by colored symbols, gray triangles are CEA's stations, blue squares demonstrate MNR's stations, and red triangles indicates open-access global stations

there is no tsunami buoys data available in the SCS region currently. Given that the deep-ocean tsunami buoys play significance roles in tsunami early warning, China has plans to redeployed the tsunami bouys in SCS.

3.3 Determination of preliminary earthquake parameters

If a large undersea earthquake occurs, quicker and more reliable preliminary earthquake parameters, such as the origin time, latitude and longitude of epicenter, focal depth and magnitude, are important to tsunami warning with a view of forecasting the tsunami threat, which is more relevant for coastal areas with possible local tsunamis.

The earthquake monitoring and processing systems, including SeisComp3 (SP3) and Antelope, were built in the SCSTAC to monitor, detect and rapidly identify possible tsunamigenic earthquakes within the Area of Service for tsunami warning, incorporating widespread data collection, data quality control, data archiving, real-time data transfer protocol, automated and interactive data processing procedures to determine origin time, location, depth, magnitudes. SeisComp is a non-commercial seismological software for data acquisition, processing, distribution and interactive analysis that has been developed by the GEOFON Program Helmholtz Centre Potsdam, GFZ German Research Centre for Geosciences and gempa GmbH (<https://www.seiscomp3.org/>). Magnitude is an essential parameter for an efficient tsunami warning system, SP3 allows rapid quantification of the size of a large earthquake, which adopts different standard magnitude scale (M_L , mb, mB, M_{wp} , M_S and others) and derived magnitudes ($M_w(mB)$, $M_w(M_{wp})$, $M(\text{summary})$, $M_w(\text{avg})$). The Antelope package is an integrated array of data collection and seismic data processing system and commercially operated by Boulder Real Time Technologies (BRIT, <http://www.britt.com>). So far, the magnitude of the earthquake measured by the Antelope software at the SCSTAC is mb, M_s and M_{wp} . For the purpose of tsunami warning, there is a significant limit to very strong tsunami-related earthquake, and the mb and M_s are constrained by frequency components and may saturate for very larger earthquake leading to underestimation of the actual magnitude, thus not suitable for tsunami warning. Since M_{wp}

and mB are not easily saturated (Tsuboi et al. 1999; Bormann and Saul 2009), they are often used to quickly determine the magnitude of major earthquake to assess the tsunami risk.

Earthquake monitoring and processing facilities at the SCSTAC play an significant role in the operation of tsunami warning and mitigation systems. A total of earthquakes of magnitude ≥ 6.0 occurred globally from January to December 2019, nine of which occurred in the SCS region. Seismic monitoring and processing results show that SP3 and Antelope systems provide stable and reliable preliminary earthquake parameters within 3–8 min after the origin time of the earthquake, providing ample time for tsunami warnings.

Furthermore, the SCSTAC receives automated and interactive earthquake information in real time from the China Earthquake Networks Center (CENC) via a dedicated cable. Meanwhile, SCSTAC operates a real-time earthquake notification service from the USGS National Earthquake Information Center (NEIC, <https://earthquake.usgs.gov>), the European Mediterranean Seismological Centre (EMSC, <https://www.emsc-csem.org>), the Japan Meteorological Agency (JMA, <http://www.jma.go.jp>), as well as information from the Pacific Tsunami Warning Center (PTWC, <https://www.tsunami.gov>), to ensure the smooth operation of the tsunami warning system.

3.4 Fast characterization of focal mechanism parameters

For tsunami warning and emergency response, it is of great importance to rapidly determine the potential tsunami threat caused by an earthquake in real time. Nevertheless, tsunami warning information only relies on the depth and magnitude of earthquake may underestimate the tsunami's potential and trigger the false alarm or potential threats to be overlooked. A real-time tsunami simulation has become one of the effective tools for tsunami forecasting with the development of tsunami warning and high performance computing technology (Titov et al. 2005; Allen and Greenslade 2008). Tsunami numerical simulation is capable of simulating the three evolution process: generation, propagation and inundation. The tsunami modeling is to provide more reliable and accurate estimate of wave arrival time, wave height and inundation area immediately following a tsunami event, providing assistance and support for the forecasting operation of tsunami warning. In the process of numerical simulation of tsunami, earthquake source parameters (seismic moment, centroid depth and location, fault plane solution, rupture area) directly affect tsunami generation as used in rapid tsunami modeling. Therefore, it is key element to analyze tsunamigenic earthquakes that includes the rapid and accurate determination of earthquake source parameters, to give better forecasting of tsunamigenic earthquakes and risk assessment of tsunami hazards in both accuracy and speed.

The W phase inversion has been testified to yield reliable earthquake source solutions and use of W phase for rapid tsunami assessment as it is a long period (100–1000 s) phase with relative rapid group velocities (4.5–9 km/s) that is faster than surface wave and the amplitude is not easy to be clipping (Kanamori and Rivera 2008; Hayes et al. 2009; Zacharie et al. 2012). The W phase can provide rapid and reliable estimates of the overall source parameters of large earthquakes for rapid assessment of tsunami potential.

The W phase source inversion algorithm is integrated to the SeisComP3 system, which provides preliminary determination of earthquake parameters, including the preliminary magnitude, source location and origin time, and real-time waveform archives. In order to prompt the efficiency of inversion, the Green's function database should be synthesized by

summation of normal modes (Woodhouse 1988) using PREM velocity model (Dziewonski and Anderson 1981) in advance for a distance range of $0^\circ \leq \Delta \leq 90^\circ$ with interval of 0.1° , for a depth range of 0–760 km, the depth interval changes with depth increasing.

W phase inversion is running and accessible at the SCSTAC for larger earthquake. Figure 7 shows the focal mechanism solutions of the W phase method for earthquakes with magnitude ≥ 6.0 from January to December in 2019. A number of practical cases show that the W phase solution calculated at SCSTAC is issued within 10–20 min of the earthquake occurrence. According to the real earthquake source parameters, the scaling relationships provided by Blaser et al. (2010) are used to estimate the width (W) and length (L) of the fault from the moment magnitude (M_w), and the center of the fault is located at the centroid of the W phase inversion. Then, an average slip amount (D) can be estimated from the surface area (A) of fault with assuming the shear modulus (μ) and seismic moment (M_0). The coseismic deformation of the seafloor surface as accurate information about the initial conditions of the tsunami is calculated in an elastic half-space with uniform isotropic elastic properties following Okada (1985), integrating 30-arc-sec GEBCO grid bathymetric data (Becker et al. 2009) to support tsunami model of the COMCOT (Cornell Multi-Grid Coupled Tsunami Model) developed by Cornell University (Liu et al. 1998; Wang 2009), which quickly estimates the arrival time and amplitude of tsunami, provides quantitative tsunami forecasting, reduces the occurrence of false alarm, and improves the reliability and accuracy of tsunami warning (Fig. 8).

3.5 Finite fault model inversion

Conventionally, a rectangular fault geometry with a simple uniform slip distribution may represent the source of a tsunamigenic earthquake, using scaling relationships related magnitude and seismic moment with fault length, width and average slip. Okada's formula (Okada 1985) is used to compute the initial coseismic seafloor displacements for tsunami forecasting modeling; in this form, complex rupture processes including non-uniform slip distribution and spatial–temporal evolution of rupture are not considered. However,

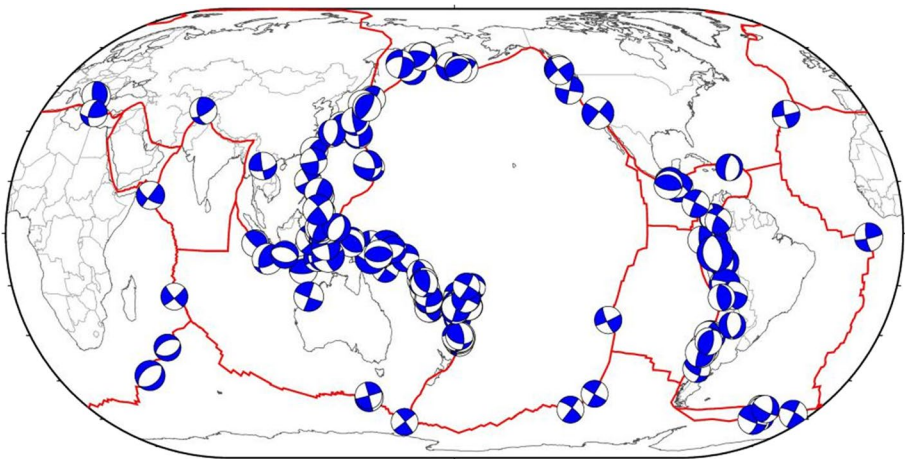


Fig. 7 Focal mechanism solutions (blue beach balls) of the earthquakes with $M \geq 6$ from January to December, 2019

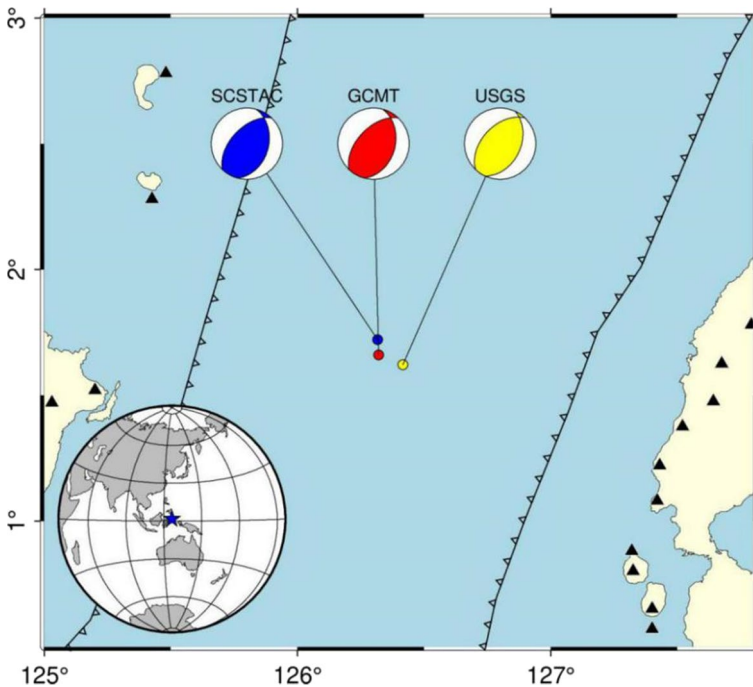


Fig. 8 Location of epicenter (circles) and focal mechanism solution of the Molucca Sea earthquake from various institutes of SCSTAC (blue), GCMT (red) and USGS (yellow). The teeth lines are the main trenches, and black triangles are volcanoes surrounding the focal areas. The blue star in the inset demonstrates the location of epicenter from SCSTAC

stochastic and heterogeneous spatial slip distribution has an important influence on tsunami numerical simulation, especially significant for local tsunamis (Goda, et al. 2016; Geist 2002; Rabinovich et al. 2008; Yamazaki et al. 2013). In addition, the source time function is important for use in identifying slow or tsunami earthquake. Tsunami warning centers can rapidly assess these types of events in tsunami alert areas.

In order to better characterize the detailed spatial and time evolution of tsunami generation, propagation and coastal inundation and reduce the influence from earthquake source model on tsunami numerical simulation, the tsunami warning centers require fast and robust finite fault source model provided by real-time waveforms after the occurrence of earthquake and improve the computational accuracy of wave prediction (Weinstein and Lundgren 2008).

Finite fault models generated by the SCSTAC are generally implementing teleseismic body-wave inversion program by Kikuchi and Kanamori (1982,1986,1991,2003; Kikuchi et al. 1993), which performs an inversion using GSN broadband P waveforms at distances 30°–90° from the real-time stream server. Before starting to the finite fault model inversion, initial length and width of fault are estimated from empirical relations with earthquake's moment magnitude (Blaser et al. 2010), and a fault rupture plane should be defined using fixed strike and dip from W phase inversion before conducting the finite fault source inversion. Since the solution to the focal mechanism consists of two nodal planes, we cannot easily determine which plane is the true seismogenic fault plane. Therefore, both nodal

planes are used for rapid finite fault slip model inversion in tsunami warning context, the fault plane with the lower misfit between observed and synthetic seismograms been considered as near-actual rupture plane for tsunami simulation.

Finite fault solution provides each subfault with variable latitude, longitude, depth, slip, rake angle and other parameters. By applying Okada's formulation to each subfault, we reconstruct the sea bed displacement with higher resolution to generate the tsunami initial condition. Only the P wave is used here on the vertical component to invert the finite fault model. If S wave or surface wave is involved in the inversion, which may take more minutes, it is difficult to fulfill the needs of near real-time tsunami warning.

4 A case study: the Molucca Sea M_w 7.1 earthquake of December 14, 2019

Since the trial operation of the South China Sea Tsunami Warning and Mitigation System on January 16, 2018, SCSTAC has released tsunami bulletins for 10 earthquakes with $M \geq 6.0$ that occurred in the responsible area of tsunami warning service. Broadcasting the tsunami information to state members takes less than 8 min after the event origin time. The accuracy of preliminary earthquake parameters on hypocenter location, depth and magnitude is within 0.3° , 30 km and 0.3 unit of magnitude, which fully meets the key performance designed indicators of the tsunami warning system.

A 15-km-deep M_w 7.1 earthquake took place in Molucca Sea, Indonesia (1.621°N , 126.416°E), on November 14, 2019, at 16:17 (UTC). The South China Sea Tsunami Advisory Center (UNESCO-IOC/SCSTAC) of the UNESCO Intergovernmental Oceanographic Commission in Beijing immediately issued a tsunami warning message to surrounding countries in the SCS region after earthquake, which generated a potential local tsunami within 300 km near the epicenter (www.scstac.org). According to sea-level data from tide gauge at costal area near the epicenter, the earthquake triggered a tsunami with wave height of 10 cm. This earthquake produced strong shaking with maximum intensity up to VI (<https://earthquake.usgs.gov/earthquakes/eventpage/us60006bjl/dyfi/intensity>). Because the epicenter of this earthquake was located in the Molucca Sea approximately 130 km from nearest coastal areas, it did not lead to casualties and losses in Molucca Sea coastal area.

The SeisComp3's real-time earthquake monitoring system provided the preliminary basic parameters of M_w 7.1 Molucca Sea earthquake immediately about 4 min 34 s after the earthquake, occurring at the epicenter of latitude 1.621°N and longitude 126.416°E with depth of 15 km. Approximately 8 min and 3 s after the event, Antelope system as a backup measured the earthquake parameters. Such earthquake parameters are consistent with each other and can be used in initial tsunami warning.

The first focal mechanism solution is made about 8 min after the earthquake with the 10 broadband waveforms by the W phase source inversion method, and it revealed that M_w 7.1 Molucca Sea earthquake occurred at a reverse-typing fault. As more stations were used in the source inversion, the more stable source parameters were obtained within 15 min after the earthquake, detailed source parameters are shown in Tab. 1. A number of focal mechanism solutions indicate that our results are stable and reliable because the result from different distance range is consistent. The focal mechanism solutions are also in line with other agencies from GCMT and USGS (Fig. 7 and Table 2). In order to better evaluate the reliability and stability of our results, the minimum 3-D spatial rotation angle proposed

Table 1 Source parameters of M_w 7.1 Molucca Sea earthquake obtained by W phase method at time lapse of earthquake



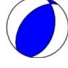
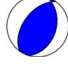
After earth-quake/min	Nodal plane I			Nodal plane II			Depth/km	M_w	Number of stations	Beach ball
	Strike/ $^\circ$	Dip/ $^\circ$	Rake/ $^\circ$	Strike/ $^\circ$	Dip/ $^\circ$	Rake/ $^\circ$				
8	219	48	107	14	45	72	23.5	7.1	10	
10	225	45	116	10	51	67	23.5	7.1	16	
12	221	49	109	14	45	70	23.5	7.1	35	
15	217	52	102	17	40	75	23.5	7.1	60	

Table 2 Comparison of the M_w 7.1 Molucca Sea earthquake source parameters from different institutes

Sources	Nodal Plane I			Nodal Plane II			Depth/km	M_w	Kagan's angles/ $^\circ$
	Strike/ $^\circ$	Dip/ $^\circ$	Rake/ $^\circ$	Strike/ $^\circ$	Dip/ $^\circ$	Rake/ $^\circ$			
GCMT	223	55	107	15	39	67	29.6	7.1	–
USGS	224	50	102	25	42	76	35.5	7.1	7.6
SCSTAC	217	52	102	17	40	75	23.5	7.1	5.9

by Kagan (1991) is a measure of the difference between two focal mechanism solutions. Kagan's angles are calculated relative to a reference mechanism from GMT solution. Table 2 shows that the Kagan's angles at a low level, indicating that there is reasonable consistency between the two sets of solution. All of the focal mechanism solutions for the event suggested that it activated a reverse faulting structure, with a moderate dip toward either the northwest or the southeast.

Two conjugate nodal planes (I: strike = 217 $^\circ$, dip = 52.0 $^\circ$, rake = 102 $^\circ$, II: strike = 17 $^\circ$, dip = 40 $^\circ$, rake = 75 $^\circ$) from W phase solutions after earthquake were used to constrain source model for finite fault inversion. We performed 55 vertical component of GSN broadband waveforms in finite fault inversion. The waveforms were processed by removing the mean, removing the instrument response, integrating to displacement, applying a band-pass filter between 0.01 to 0.5 Hz and resampling the time series to 0.01 s/sample. The Green function has been computed with 1D IASPEI91 velocity model using a Kikuchi and Kanamori method, the Green function where filtered with the same band applied to the data.

We used a total number of 56 subfaults with a unit area of 5 km \times 5 km in a 8 (along strike) \times 7 (along dip) grid for teleseismic inversions, and the fault length and width are 40 km and 35 km. A rupture velocity of 2.5 km/s, the factor of 1.0 was assumed.

The correlation between observed and synthetic waveforms was quantified using root mean square (RMS) misfit. After comparing waveform fits based on the two planes of the focal mechanism solution, we find that the first nodal plane with SSW trending (

strike = 217°, dip = 52°, RMS = 0.225) fits the data better than the second nodal plane with NNE trending (strike = 17°, dip = 40°, RMS = 0.253). The fault plane with strike = 217° was considered as the actual seismogenic fault for tsunami simulation. The slip area was concentrated at 35 km (along strike) × 30 km (along dip) with an average slip of 4.0 m, located close to the epicenter. We obtained a seismic moment of 4.6×10^{20} N·m equivalent to $M_W = 7.0$. The source time functions are also shown in Fig. 9, this event was shorter than ~17 s, and seismic moment quickly released after the rupture began, occurred peak about 5 s after earthquake and healed after 15 s of earthquake.

Since the slip distribution inversion on an unknown fault is highly nonlinear and unresolved, the primary sources of uncertainty are mainly from incomplete and noisy data, model error, parameterization assumptions and choices. A number of studies have been conducted to investigate these non-uniqueness and uncertainty issues using various datasets (Sarao et al. 1998; Delouis et al. 2002; Zhang et al. 2015), different crustal velocity

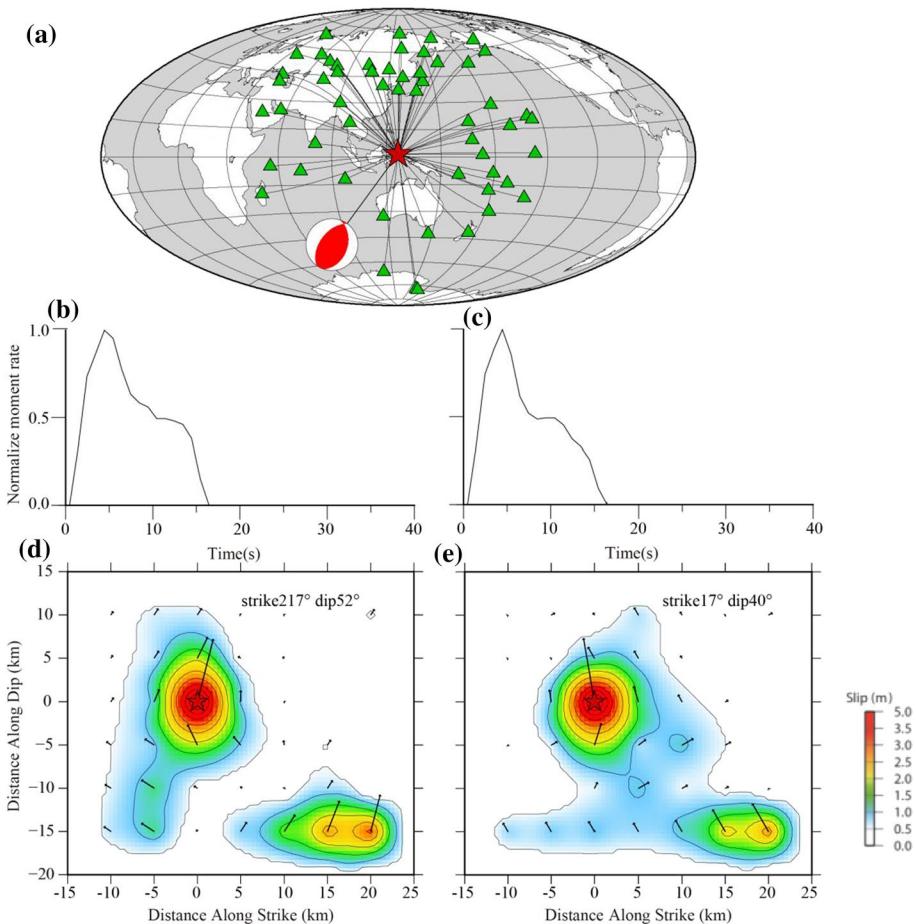


Fig. 9 Finite fault model of the Molucca Sea earthquake Seismic stations (green triangle) used in finite fault model inversion; **b, c** and **d, e** source time function and slip distribution in the rectangular finite fault model inverted from two conjugate nodal planes, respectively. The focal mechanism solution of the Molucca Sea earthquake was derived from W phase faster inversion

structure (Graves and Wald 2001) and incorrect parameter assumptions in the inversions (Beresnev 2003). Due to the purpose of fast tsunami computation with the near real-time finite fault model solution, the uncertainties of finite fault model solutions do not consider in our paper.

The sea-level observation data from tide gauges lie at the coast lines near the epicenter of Malucca Sea M_w 7.1 earthquake, including Bitung, Ternate, Jailolo and Tidore gauge stations, which show that a small-scale tsunami generated after occurrence of the earthquake. The sea-level history records at the tide gauges, in addition to tsunami wave, also include tide waves and abnormal disturbances in sea level; in order to better describe and identify the tsunami wave, we use a band-pass filter (2–120 min) to separate the tsunami wave from original signal, the same filter also for tsunami simulation waveform at each station.

The variance reduction VR value evaluates the waveform fit between the observed and synthetic tsunami wave, a good fitting with a higher VR value, which is calculated using the following formula:

$$VR = 1 - \frac{\sum (o - s)^2}{\sum o^2}$$

where o and s represent the observed and synthetic tsunami wave of the tide station.

The tsunami waves propagate to the near shore zone and run up on the beach, nonlinear effects become prominent as the water gets shallower, water level changes strongly affected by local topography and bathymetry of the coast. It is often difficult or even impossible to accurately simulate the full wave trains for a tsunami event. Therefore, the observed first wave cycle is often compared with the synthetic computed using tsunami numerical model.

In order to examine whether the W phase and finite fault solutions are valid in tsunami forecasting models, the tide gauge observations (black lines) for the Molucca Sea tsunami event are used to compare with the model predictions based on uniform slip model from W phase (red lines) and heterogeneous slip model from finite fault solutions (blue lines), as shown in Fig. 10. It can be seen from the plots that the predictions from both type of models match the observed tsunami data better except for the Bitung tide gauge station, due to the Bitung station located at the trumpet-shaped bay connecting with the Molucca Sea, when the tsunami waves propagate to the bay, and leading to the continuous reflection and interference, which has a significant amplifying effect on the tsunami wave. Therefore, there are significant differences between the observed and synthetic waveform recorded by the Bitung station. The VR values of the other stations are all above 0.6, and the prediction maximum wave amplitude and arrival time are relatively consistent with the tsunami data. Comparing the different type of fault model, the simplified uniform slip model has slightly larger prediction errors than the finite fault model, but the prediction errors caused by neglecting slip heterogeneity are insignificant for rapid tsunami early warning.

5 Summary and discussion

South China Sea region is situated at the intersection of the Eurasian Plate, the Pacific Plate and the India–Australia Plate. The dynamic complex interaction between plates triggers high frequency earthquake and tsunami activities on the northern margin of the South China Sea region. Historical earthquake and tsunami records indicate that tsunami threat is

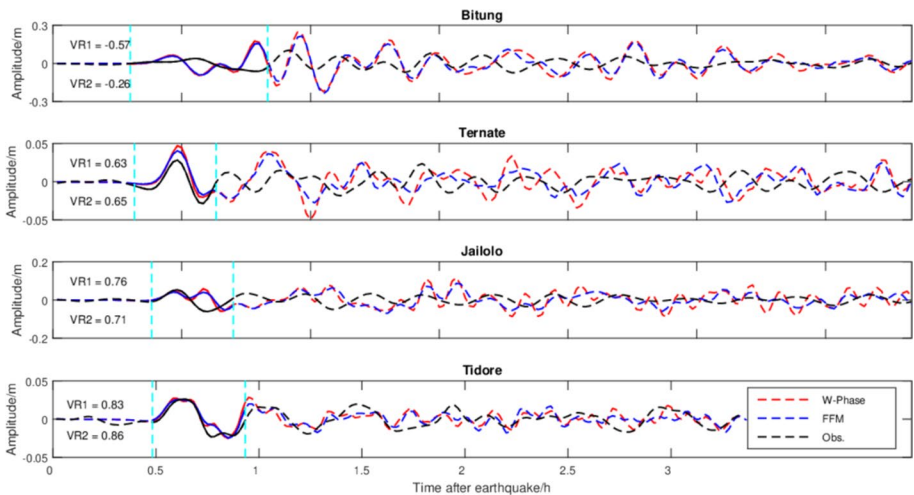


Fig. 10 Waveform comparison of observed recorded by tide gauges and its synthetic computed using different type of fault model. The tide gauge observations (black lines) for the Molucca Sea tsunami event are used to compare with the model predictions based on uniform slip model from W phase (red lines) and heterogeneous slip model from finite fault model (blue lines). The values of VR1 and VR2 represent the waveform fitting for the first observed wave cycle compared with predicted wave based on W phase and finite fault model at specified time windows

highly probable at the eastern edges of the Sunda Plate, including the Manila Trench, the Negros Trench, the Sulu Trench and the Cotabato Trench and the North Sulawesi Trench.

The full operation of the South China Sea Tsunami Advisory Center ensures a significant guarantee in reducing tsunami risk and the protection of people's lives and properties within the South China Sea region. The sophisticated real-time earthquake monitoring system collects data from seismic stations or servers and performs the processing to detect and analyze earthquakes, providing fast accurate and reliable preliminary earthquake parameters, focal mechanism solution and finite fault model for the areas of responsibility of the SCSTAC. Great strides have been taken to promote the development of tsunami warning system. There are important practical consequences for marine hazard prevention and mitigation.

The real-time earthquake monitoring and processing system of SCSTAC has been continuously operating since its trial operation in 2018. A wide range of practical applications in tsunami warning have proved that the real-time earthquake monitoring system provides rapid, fast preliminary earthquakes parameters within 3–8 min, and near real-time determination of earthquake source parameters including moment magnitude, centroid location and depth, strike, dip, rake and others within 10–20 min after the earthquake. This system also provides finite fault model solutions and earthquake duration with teleseismic body-wave slip distribution inversion for the tsunami warning, which are obtained typically less than 30 min after origin time.

In order to further promote the earthquake and tsunami monitoring and warning capabilities of the SCS region, The member states of SCS launched an initiative at the 6th meeting of SCS Working Group held in Shanghai, China, for the establishment of the core observations network of seismic and sea-level stations in the SCS region with

115 seismic stations and 69 tide gauge stations, and all the shared data are dedicated for tsunami warning service. The shared servers of seismic and sea-level data are set up in SCSTAC, and the tsunami warning centers of member states from the SCS region request the shared data via the specified users and passwords.

Note that it remains an open science question how to decide quickly and reliably whether a major undersea earthquake could trigger a tsunami after it occurrence. Although scientists have seen some tsunami patterns in previous earthquakes, the relationship between earthquakes and tsunamis remains unclear to many people, and tsunami warning are still facing enormous challenges. In future, SCSTAC will develop state-of-the-art ways for seismological tsunami warning. For example, slow earthquakes can rapidly be detected (Newman and Okal 1998), the back array projection method for rapid estimation of earthquake rupture scale and direction (Wang et al. 2017), as well as fast earthquake magnitude estimation using P wave duration (Lomax and Michelini 2011). These methods will also reinforce and strengthen the current real-time earthquake monitoring and processing system, and such system may enable more effective for tsunami warning service.

Acknowledgements Great thanks to the aid, assistance and support from IOC/UNESCO, the Intergovernmental Coordination Group for the Pacific Tsunami Warning and Mitigation System, the Pacific Tsunami Warning Center, the Northwest Pacific Tsunami Advisory Center, the tsunami warning centers surrounding the South China Sea region, as well as the China Earthquake Administration during the process of establishment and operation of the SCSTAC. Thanks to Gempa of Germany and BRTT of the USA for the earthquake monitoring and processing system, thanks to IRIS/DMC, GEOPHONE and GEOSCOPE for providing the real-time seismic waveforms, and thanks to Luis Rivera for the W phase inversion program and Kikuchi for the teleseismic body-wave inversion program. We used the GMT software for drawing the figures. This study was supported by State Key Laboratory of Marine Geology, Tongji University (No. MGK202004).

References

- Allen SCR, Greenslade DJM (2008) Developing tsunami warnings from numerical model output. *Nat Hazards* 46(1):35–52
- Athukorala PC, Resosudarmo BP (2005) The Indian Ocean tsunami: economic impact, disaster management and lessons. *Asian Econ Pap* 4(1):1–39
- Aurelio MA, Dianala JDB, Taguibao KJL, Pastoriza L, Reyes K, Sarande R, Lucero A (2017) Seismotectonics of the 6 February 2012 MW 6.7 Negros earthquake, central Philippines. *J Asian Earth Sci* 142:93–108
- Aziz M, Shibazaki B, Fujii Y (2011) Tsunami numerical simulation around Sulu sea and Celebes sea. *Bulletin of the International Institute of Seismology and Earthquake Engineering*, pp 1–50
- Baeda YA (2011) Seismic and Tsunami Hazard Potential in Sulawesi Island. *Indo J Int Dev Cooper* 17(1):17–30
- Becker JJ, Sandwell DT, Smith WHF, Braud J, Binder B, Depner JL, Ladner R (2009) Global bathymetry and elevation data at 30 arc seconds resolution: SRTM30_PLUS. *Mar Geodesy* 32(4):355–371
- Beresnev IA (2003) Uncertainties in finite-fault slip inversions: to what extent to believe? (a critical review). *Bull Seismol Soc Am* 93(6):2445–2458
- Bird P (2003) An updated digital model of plate boundaries. *Geochem Geophys Geosyst* 4:1027. <https://doi.org/10.1029/2001GC000252>
- Blaser L, Krüger F, Ohrnberger M, Scherbaum F (2010) Scaling relations of earthquake source parameter estimates with special focus on subduction environment. *Bull Seismol Soc Am* 100(6):2914–2926
- Bormann P, Saul J (2009) A fast, non-saturating point estimator for great earthquakes. *Seismol Res Lett* 80(5):808–816
- Cardwell RK, Isacks BL, Karig DE (1980) The spatial distribution of earthquakes, focal mechanism solutions, and subducted lithosphere in the Philippine and northeastern Indonesian island. In: Hayes DE

- (ed) *The Tectonic and Geological Evolution of Southeast Asian Seas and Islands*, Geophysics Monograph (Series 23). AGU, Washington, pp 1–35
- Cardwell RK, Isacks BL (1978) Geometry of the subducted lithosphere beneath the Banda Sea in eastern Indonesia from seismicity and fault plane solutions. *J Geophys Res Solid Earth* 83:2825–2838
- Delouis B, Giardini D, Lundgren P, Salichon J (2002) Joint inversion of InSAR, GPS, teleseismic, and strong-motion data for the spatial and temporal distribution of earthquake slip: application to the 1999 Izmit Mainshock. *Bull Seismol Soc Am* 92(1):278–299
- Dziewonski AM, Anderson DL (1981) Preliminary reference Earth model. *Phys Earth Planet Inter* 25:297–356
- Frohlich C (1992) Triangle diagrams: ternary graphs to display similarity and diversity of earthquake focal panels. *Phys Earth Planet Inter* 75(1–3):0–198
- Geist EL (2002) Complex earthquake rupture and local tsunamis. *J Geophys Res* 107(B5):2086
- Goda K, Yasuda T, Mori N, Maruyama T (2016) New scaling relationships of earthquake source parameters for stochastic tsunami simulation. *Coast Eng J* 58(3):1650010
- Graves R, Wald D (2001) Resolution analysis of finite fault source inversion using one and three-dimensional Green's functions: 1. Strong motions. *J Geophys Res: Solid Earth* 106(B5):8745–8766
- Hayes GP, Rivera L, Kanamori H (2009) Source inversion of the w-phase: real-time implementation and extension to low magnitudes. *Seismol Res Lett* 80(5):817–822
- Imamura F, Synolakis CE, Gica E, Titov V, Lee HJ (1995) Field survey of the 1994 mindoro island, Philippines tsunami. *Pure Appl Geophys* 144(3):875–890
- Johnston CR, Bowin CO (1981) Crustal reactions resulting from the mid-Pliocene to recent continent-island arc collision in the Timor region. *BMR J Austral Geol Geophys* 6:223–243
- Kagan YY (1991) 3-D rotation of double-couple earthquake sources. *Geophys J Int* 106(3):709–716
- Kanamori H, Rivera L (2008) Source inversion of W phase: speeding up seismic tomography warning. *Geophys J Int* 175(1):222–238
- Kikuchi M, Kanamori H (1986) Inversion of complex body waves-II. *Phys Earth Planet Inter* 43:205–222
- Kikuchi M, Kanamori H (1982) Inversion of complex body waves. *Bull Seismol Soc Am* 72:491–506
- Kikuchi M, Kanamori H (1991) Inversion of complex body waves—III. *Bull Seismol Soc Am* 81:2335–2350
- Kikuchi M, Kanamori H (2003) Note on teleseismic body wave inversion program. The Earthquake Research Institute, Tokyo University, Japan. Online at <http://www.eri.u-tokyo.ac.jp/ETAL/KIKUCHI/>
- Kikuchi M, Kanamori H, Satake K (1993) Source complexity of the 1988 Armenian Earthquake: evidence for a slow after-slip event. *J Geophys Res* 98:15797–15808
- Kirby S, Geist E, Lee WHK, Scholl D, Blakely R (2005) Tsunami source characterization for western pacific subduction zones: an optimization report. In: *DART Network Optimization: 2005 Workshop Report*: NOAA Technical Memorandum ERL PMEL
- Kreemer C, Holt WE, Goes S, Govers R (2000) Active deformation in eastern Indonesia and the Philippines from GPS and seismicity data. *J Geophys Res* 105(B1):663
- Lay T (2005) The Great Sumatra-Andaman Earthquake of 26 December 2004. *Science* 308(5725):1127–1133
- Lin JY, Sibuet JC, Hsu SK, Wu WN (2014) Could a Sumatra-like megathrust earthquake occur in the south ryukyu subduction zone? *Earth Planets Space* 66(1):49
- Liu PL-F, Wang XM, Salisbury AJ (2009) Tsunami hazard and early warning system in South China Sea. *J Asian Earth Sci* 36(1):0–12
- Liu PL-F, Woo SB, Cho Y (1998) Computer designed for Tsunami Propagation and Inundation. Cornell University, Sponsored by the National Science Foundation, 104.
- Liu Y, Santos A, Wang SM, Shi Y, Liu H, Yuen DA (2015) Tsunami hazards along Chinese coast from potential disasters in south China sea. *Phys Earth Planet Inter* 163(1):233–244
- Lomax A, Michelini A (2011) Tsunami early warning using earthquake, duration and p-wave dominant period: the importance of length and depth of faulting. *Geophys J Int* 185(1):283–291
- Mardi NH, Malek MA, Liew MS (2017) Tsunami simulation due to seaquake at Manila Trench and Sulu Trench. *Nat Hazards* 85:1723–1741
- Megawati K, Shaw F, Sieh K, Huang Z, Wu TR, Lin Y, Tan SK, Pan TC (2009) Tsunami hazard from the subduction megathrust of the south China sea: Part I. Source characterization and the resulting tsunami. *J Asian Earth Sci* 36(1):0–20
- Michel G, Becker M, Angermann D, Reiger C, Reinhart E (2000) Crustal motion in e-and se-asia from GPS measurements. *Earth Planets Space* 52:713e720
- National Geophysical Data Center of National Oceanic and Atmospheric Administration (n/d, NGDC database): Historical Tsunami database from 2000b. c. to present, available at:<http://www.ngdc.noaa.gov/hazard/tsudb.SHTML>. Accessed March 2020

- Newman A, Okal EA (1998) Teleseismic estimates of radiated seismic energy: the E/M0 discriminant for tsunami earthquakes. *J Geophys Res Solid Earth* 103(B11):26,885–26,898
- Novosibirsk Tsunami Laboratory (n/d, NTL database): Historical Tsunami Databases for the World Ocean from 1628 B.C. to present, available at: <http://tsun.sccc.ru/OnlineCat.HTML>. Accessed March 2020
- Okada Y (1985) Surface deformation due to shear and tensile faults in a half-space. *Bull Seismol Soc Am* 75:1135–1154
- Pararas-Carayannis G (2013) The Great tohoku-oki Earthquake and Tsunami of March 11, 2011 in Japan. *Pure Appl Geophys* 171(12):3257–3278
- Rabinovich AB, Lobkovsky LI, Fine IV, Thomson RE, Ivelskaya TN, Kulikov EA (2008) Near-source observations and modeling of the Kuril Islands tsunamis of 15 November 2006 and 13 January 2007. *Adv Geosciences* 14:105–116
- Sarao A, Das S, Suhadolc P (1998) Effect of non-uniform station coverage on the inversion for earthquake rupture history for a Haskell-type source model. *J Seismol* 2(1):1–25
- Simons WJF, Socquet A, Vigny C, Ambrosius BAC, Haji Abu S, Promthong C, Subarya C, Sarsito DA, Matheussen S, Morgan P, Spakman W (2007) A decade of GPS in Southeast Asia: resolving Sundaland motion and boundaries. *J Geophys Res: Solid Earth* 112(B6):623–626
- Simons WJF, Ambrosius BAC, Noomen R, Angermann D, Wilson PM, Becker E, Reinhart A, Walpersdorf Vigny C (1999) Observing plate motions in SE Asia: Geodetic results of the GEODYSSSEA project. *Geophys Res Lett* 26:2081–2084
- Socquet A, Simons W, Vigny C, McCaffrey R, Subarya C, Sarsito D, Ambrosius B, Spakman W (2006) Microblock rotations and fault coupling in SE Asia triple junction (Sulawesi, Indonesia) from GPS and earthquake slip vector data. *J Geophys Res* 111(B8):B08409
- Syamsidik B, Umar M, Margaglio G, Fitriyansyah A (2009) Post-tsunami survey of the 28 September 2018 tsunami near Palu Bay in Central Sulawesi. *Indo: Int J Disas Risk Reduct* 38:101229
- Titov VV, Gonzalez FI, Bernard EN, Eble MC, Venturato AJ (2005) Real-time tsunami forecasting: challenges and solutions. *Nat Hazards* 35(1):35–41
- Tsuijboi S, Whitmore PM, Solokowski TJ (1999) Application of *Mwp* to deep and teleseismic earthquakes. *Bull Seismol Soc Am* 89(1):1345–1351
- Wang D, Kawakatsu H, Zhuang J, Mori J, Maeda T, Tsuruoka H, Zhao X (2017) Automated determination of magnitude and source length of large earthquakes using backprojection and P wave amplitudes. *Geophys Res Lett* 44(11):5447–5456
- Wang XM, Liu PL-F (2006) An analysis of 2004 Sumatra earthquake fault plane mechanism and Indian Ocean tsunami. *J Hydraul Res* 44(2):147–154
- Wang XM (2009) Technical document for COMCOT v.1.7. Institute of Geological and Nuclear Science, New Zealand
- Weinstein SA, Lundgren PR (2008) Finite fault modeling in a tsunami warning center context. *Pure Appl Geophys* 165:451–474
- Woodhouse JH (1988) The calculation of Eigen frequencies and Eigen functions of the free oscillations of the earth and the sun. In: Doornbos DJ (ed) *Seismological algorithms, computational methods and computer programs*. Academic Press, London, pp 321–370
- Xie X, Chen C, Li L, Wu S, Yuen D, Wang D (2019) Tsunami hazard assessment for atoll islands inside the south China sea: a case study of the Xisha archipelago. *Phys Earth Planet Inter* 290(1):20–35
- Yamazaki Y, Cheung K, Lay T (2013) Modeling of the (2011) Tohoku near-field tsunami from finite-fault inversion of seismic waves. *Bull Seismol Soc Am* 103(2B):1444–1455
- Yang YQ, Lin YS (1990) Coastal fault and historical earthquakes at the Quanshan zone. *South China J Seismol* 1:50–55 (In Chinese)
- Zacharie D, Luis R, Hiroo K, Gavin H (2012) W phase source inversion for moderate to large earthquakes (1990–2010). *Geophys J Int* 189(2):1125–1147
- Zhang Y, Dalguer LA, Song SG, Clinton J (2015) Evaluating the effect of network density and geometric distribution on kinematic source inversion models. *Geophys J Int* 200(1):1–16
- Zhao L, Yu F, Hou J, Wang P, Fan T (2013) The role of tsunami buoy played in tsunami warning and its application in South China Sea. *Theor Appl Mech Lett* 3(3):032002

Authors and Affiliations

Zhiguo Xu^{1,2} · Shanshan Liang³ · Mohd Nashriq Bin Abd Rahman⁴ · Hongwei Li¹ · Jianyu Shi¹

✉ Shanshan Liang
liangshanshan@seis.ac.cn

¹ National Marine Environmental Forecasting Center, Beijing 100081, China

² Key Laboratory of Computational Geodynamics, University of Chinese Academy of Sciences, Beijing 100049, China

³ China Earthquake Networks Center, Beijing 100045, China

⁴ Malaysian Meteorological Department, Jalan Sultan, Petaling Jaya, 46667 Selangor, Malaysia